Surface band bending and carrier dynamics in colloidal quantum dot solids– supporting information

Pip C. J. Clark*,[a], Nathan K. Lewis[a], Jack Chun-Ren Ke[a], Ruben Ahumada-Lazo[a], Qian Chen[b], Darren C. J. Neo[c,†], E. Ashley Gaulding[d], Gregory F. Pach[d], Igor Pis[e,f], Mathieu G. Silly[g], Wendy R. Flavell*,[a].

Core level XPS showing residual Cd on CQDs synthesised by cation exchange

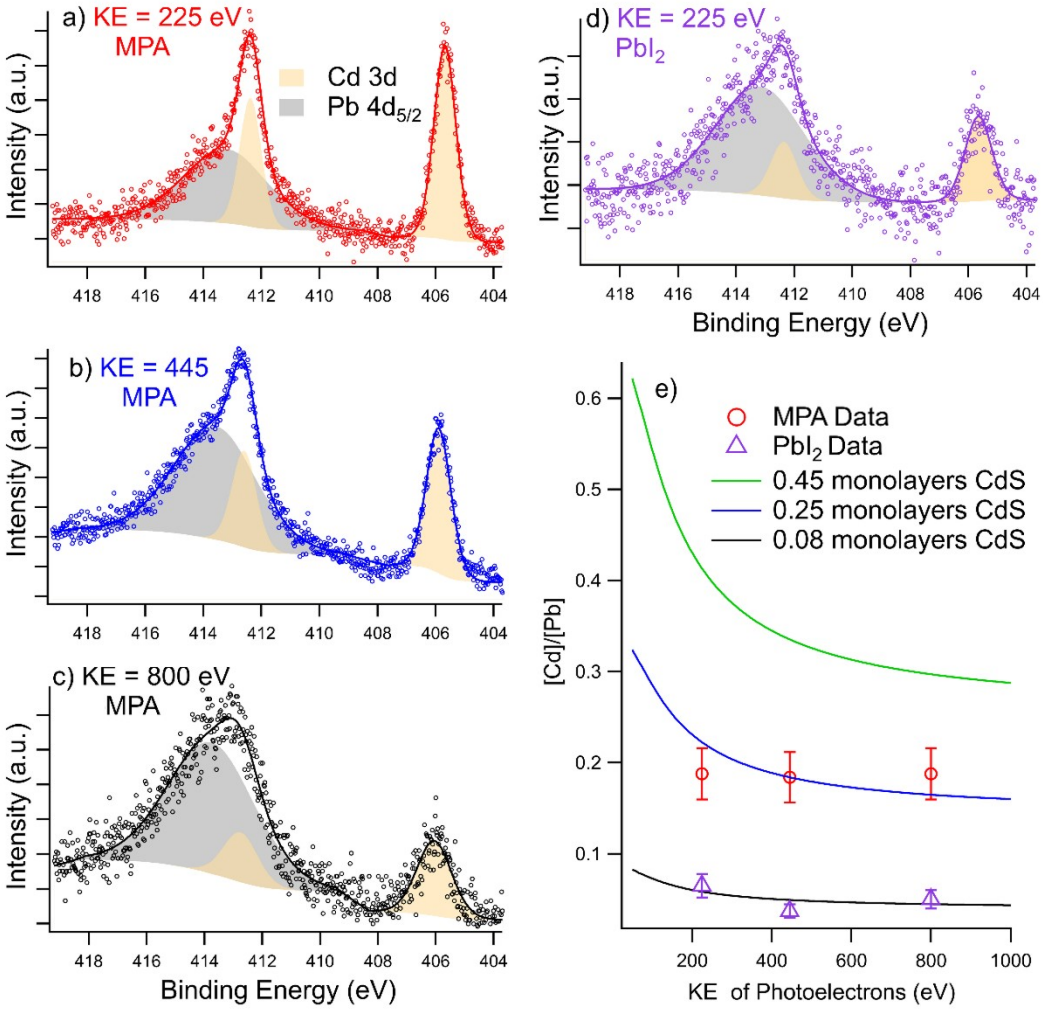

Figure S1. XPS spectra of the Pb 4d and Cd 3d regions at three of the measured photoelectron kinetic energies for the PbS-MPA CQD solid (a-c) with corresponding probing-depths of 1.2, 1.55 and 1.8 nm for the 225, 445, and 800 eV electrons respectively. d) The Pb 4d and Cd 3d region for at 225 eV KE (1.2 nm probing depth) for the PbS-PbI_2 CQD solid. e) the cross section-corrected ratios at each kinetic energy (KE) for the PbS-MPA and PbS-PbI_2 solids, and calculated ratios for different Cd thicknesses on the surface of the CQDs.[1]

Representative core level spectra of the cation-exchanged CQDs are shown in Figure S1. The best fit to the depth-profile data shown for the PbS-MPA film is consistent with either ¼ of a monolayer of

residual Cd remaining on the CQD surfaces after the synthesis (1:3 Cd:Pb ratio on the surface), or with a constant 20:80 Cd:Pb ratio present throughout the CQDs. For PbS-PbI_2 a lower amount of residual Cd is found, corresponding either to 1/12 of a monolayer on the surface (1:11 Cd:Pb ratio) or to a 5:95 Cd:Pb ratio throughout the CQD. Since the ligand exchange procedure is known to affect the amount of residual Cd at the surface of these cation-exchange-synthesised samples[2] it is probable that the Cd is located on the surface of these CQDs. In Figure S1e we use the methods for determining Cd surface content developed by Clark *et al.*[3]

Optical absorption spectra

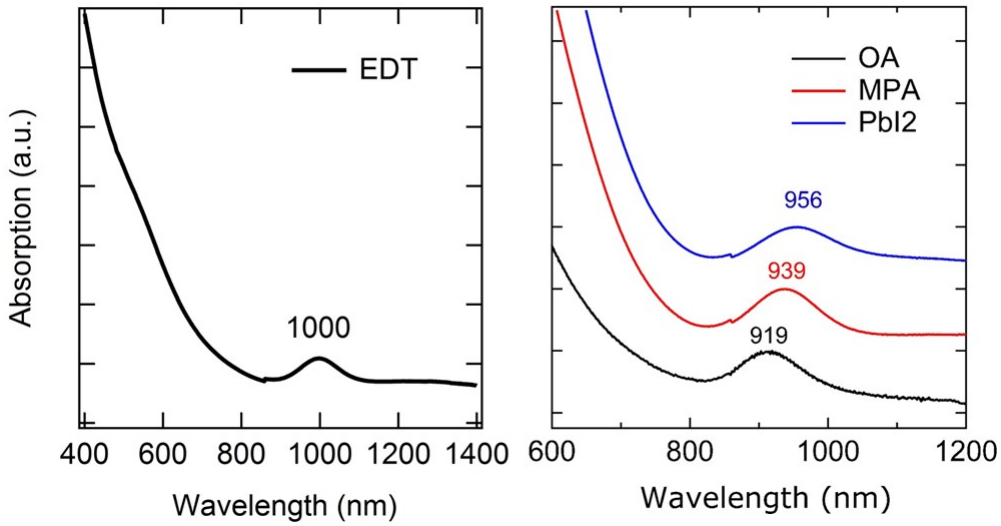

Figure S2. Optical absorbance spectra for PbS CQD solids treated with EDT (left), MPA and PbI_2 (middle), and the original ligands OA (middle). The position of the 1S absorption peak is noted for each case.

Valence band photoemission

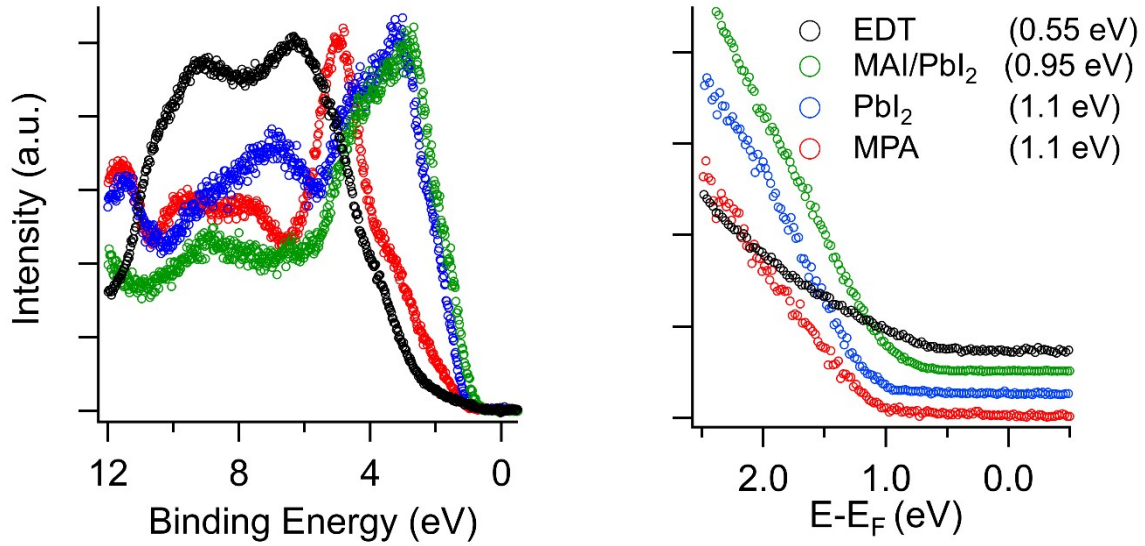

Figure S3. Photoemission of the valence band for four PbS CQD solids with different surface treatments, the right-hand side shows an expansion close to the Fermi level, with the spectra vertically offset for clarity. The energy offset between the valence band maxima and the Fermi level is indicated in brackets in the legend. The EDT sample was measured with a photon energy of 45 eV on the BACH beamline, at Elettra, while the other samples were measured at 100 eV on the

TEMPO beamline, at SOLEIL. The difference in photoionisation cross sections of VB states at the two photon energies is the cause of the major difference in appearance of the VB of EDT treated sample compared to the other samples.

Core level spectra for the samples used for static and time-resolved SPV measurements

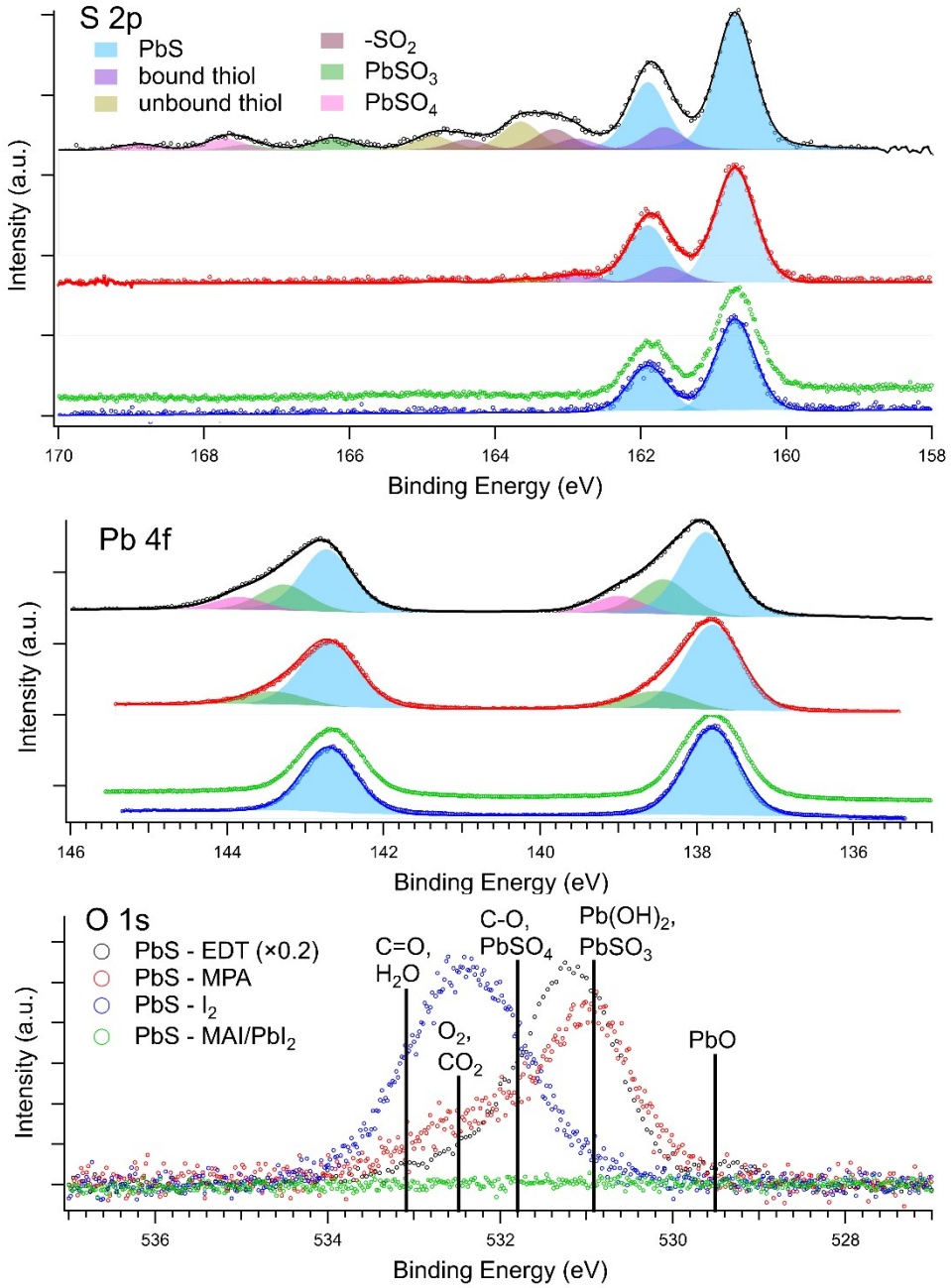

Figure S4. S 2p, Pb 4f and O 1s XPS spectra for the PbS-EDT (black), PbS-MPA (red), PbS-PbI_2 (blue) and PbS-MAI/PbI_2 (green) CQD solids with fitted components. The O 1s X-ray photoelectron spectra were normalised to the Pb 4f PbS component. The photon energies used were 475 eV for the S 2p and Pb 4f and 862 eV for the O 1s. The binding energy positions of possible species that can be found in PbS CQD films are marked on the O 1s spectra.

The S 2p spectrum for the PbS-EDT films studied with static light on/off measurements shows signs of oxidation as well as bound and unbound thiols, assignments are given in table S1. The S 2p spectra for the 3 samples studied with time-resolved XPS show only PbS present in the PbS-PbI_2 and PbS-MAI/PbI_2 solids, and the presence of bound and unbound thiol species from the 3-MPA in the PbS-MPA solid. Again in the Pb 4f spectra for PbS-PbI_2 and PbS-MAI/PbI_2 a single peak assigned to PbS or PbI_2 is present. For the PbS-MPA solid a small amount of $Pb(OH)_2$ or $PbSO_3$ is present, and in PbS-EDT a larger $Pb(OH)_2$ or $PbSO_3$ component plus $PbSO_4$ is present. This is corroborated in the O 1s

spectrum at ~531 eV where $Pb(OH)_2$ and $PbSO_3$ are expected. Importantly to understanding the time-resolved XPS results, there is also some intensity in the O 1s region that can be assigned to adsorbed O_2 and H_2O as well as oxidized carbon in both the PbS-MPA and PbS-PbI_2 solids.[4–8] There is a negligible intensity in the O 1s region from the PbS-MAI/PbI_2 solid, due to a much lower level of oxygen contamination in the film.

Table S1. XPS peak assignments for the S 2p region.

Core level	Literature Binding Energy	Observed Binding Energy (eV)
PbS	160.7[9,10]	160.7±0.1
Bound thiol	161.7[6,10,11]	161.7±0.1
Unbound thiol	163.4-6[11,12]	163.5±0.1
-SO_2	163.15[13,14]	163.2±0.1
$PbSO_3$	166.4[3,13,14]	166.2±0.2
$PbSO_4$	167-8[3,13]	167.8±0.2

Pb 5d Fit from PbS EDT films in static white-light measurements

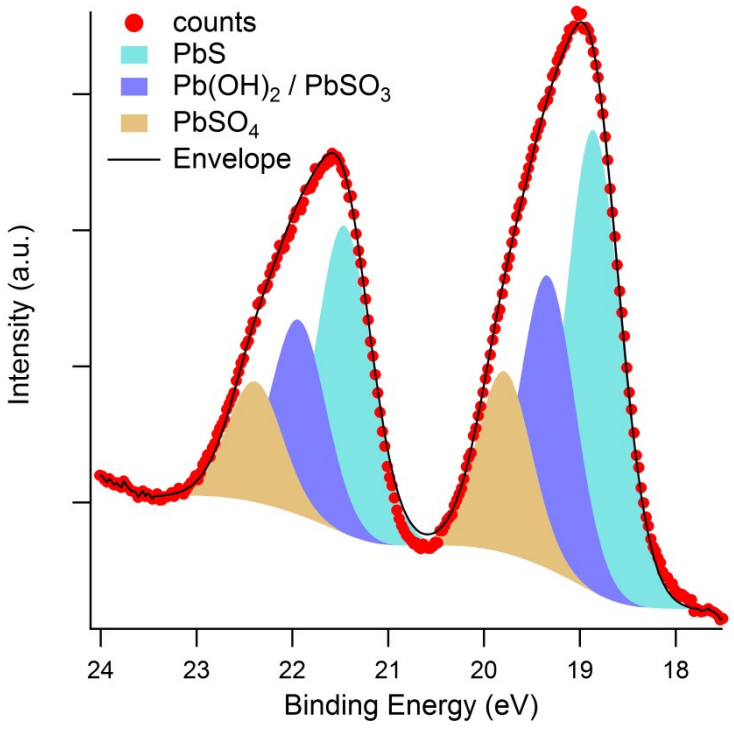

Figure S5. Pb 5d X-ray Photoelectron spectrum for the 45 nm thick PbS-EDT CQD film after storage and transfer to UHV in an N_2 environment. The photon energy used was 45 eV. The binding energies and chemical shifts for each component are listed in the text.

The fitted Pb 5d XPS spectrum in Figure S4 shows 3 components relating to PbS (18.9 eV), $PbSO_3$/$Pb(OH)_2$ (19.3, +0.4 eV from PbS), and $PbSO_4$ (19.8, +0.9 eV from PbS). These agree with binding energy shifts and values found in the literature, and also the observed degradation

mechanisms in PbS nanoparticles.[3,13,15] The ratios of these components are different to those observed in the S 2p and Pb 4f spectra shown Figure S4. This is due to the different kinetic energies of the photoelectrons used in recording each spectrum, and therefore different sampling depths (the Pb 5d spectrum was more surface sensitive than S 2p).

Cross sectional SEM and EDX

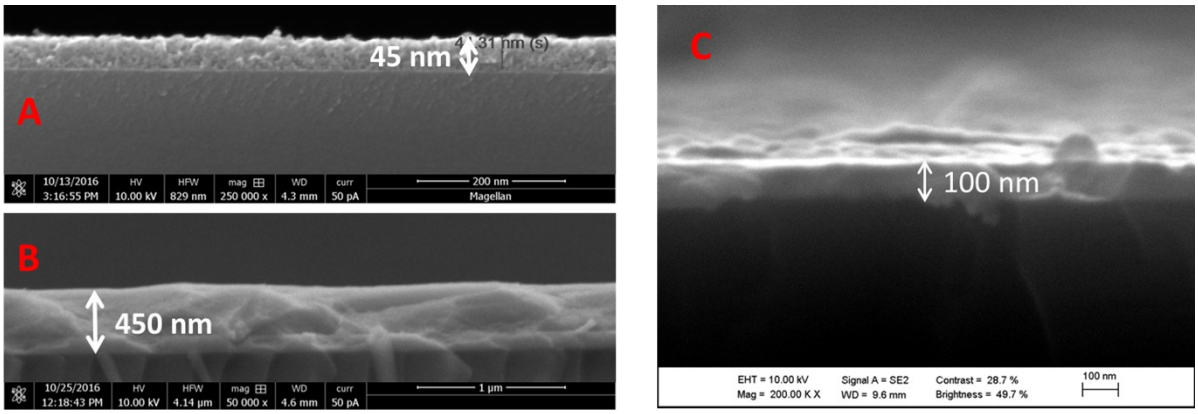

Figure S6. Cross sectional images of (A) PbS EDT CQD solid (thin), (B) PbS EDT CQD solid (thick), (C) PbS MPA CQD solid. The film thicknesses are indicated.

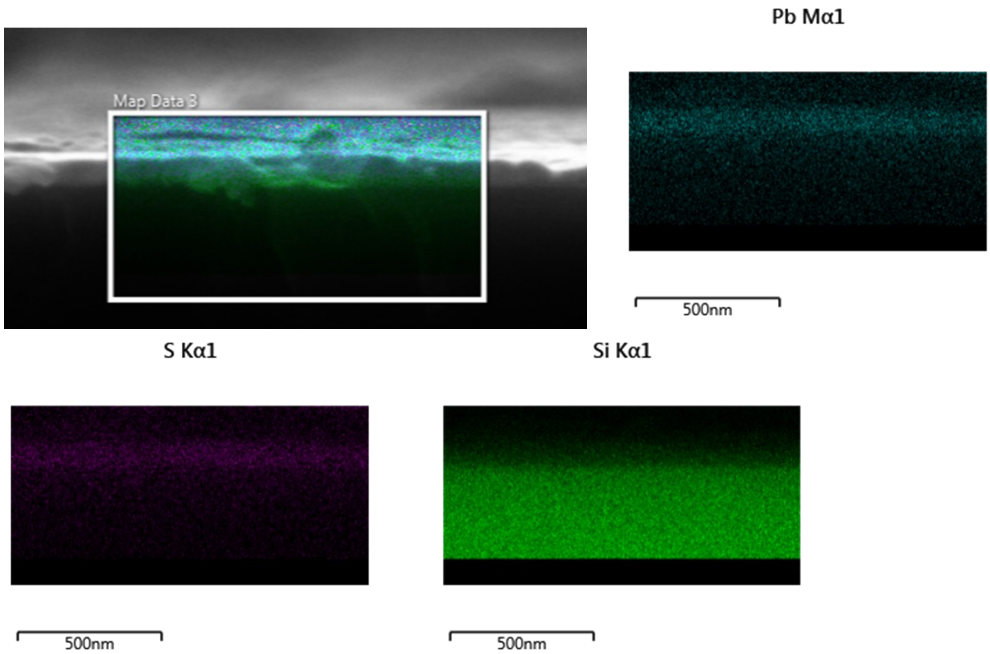

Figure S7. Cross sectional SEM images with EDX elemental mapping for Pb, S and Si in the PbS MPA CQD solid film, showing that S and Pb are only present in the 100 nm thick region at the surface of the sample.

Surface photovoltage transients - further analysis

To further analyze the surface photovoltage transients, linear fits were made to the first few points of the transient after changing from a dark steady-state to light on, and from the illuminated steady-state to light off, as shown in Figure S7. The negative ratio (light off over light on) of these two gradients is termed *C.* From algebraic manipulation of the rate of change of surface state occupation at these two conditions, it has been shown that the steady-state band bending in the dark is related to *C* and ΔV (the total SPV shift) by $V_0 = {\Delta V}/{1 - C}$.[16–18] This is a simple model design to apply to excitation in one band, applicable where the illumination is low enough that the free carrier combination does not change appreciably, and assumes that during the initial rise of the SPV shift upon light illumination there is no recombination of carriers contributing to the SPV shift.

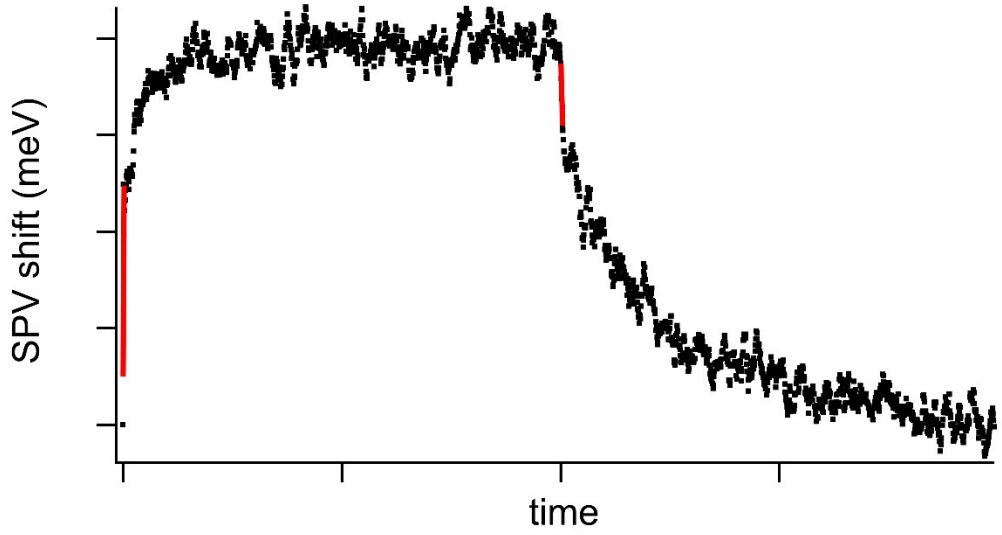

Figure S8. Example of linear fits (red) to a surface photovoltage transient when transitioning from steady-state dark and steady-state light conditions.

References

1 A. G. Shard, J. Wang and S. J. Spencer, *Surf. Interface Anal.*, 2009, **41**, 541–548.

2 P. C. J. Clark, D. C. J. Neo, R. Ahumada-Lazo, A. I. Williamson, I. Pis, S. Nappini, A. A. R. Watt and W. R. Flavell, *Langmuir*, 2018, **34**, 8887–8897.

3 P. C. J. Clark, H. Radtke, A. Pengpad, A. I. Williamson, B. F. Spencer, J. O. Hardman, M. A. Leontiadou, D. C. J. Neo, S. M. Fairclough, A. A. R. Watt, I. Pis, S. Nappini, F. Bondino, E. Magnano, K. Schulte, M. Silly, F. Sirotti and W. R. Flavell, *Nanoscale*, 2017, **9**, 6056–6067.

4 H. Heinemann, G. A. Somorjaf and B. Marchon, 1988, **26**, 507–514.

5 M.-J. Choi, J. Oh, J.-K. Yoo, J. Choi, D. M. Sim and Y. S. Jung, *Energy Environ. Sci.*, 2014, **7**, 3052.

6 Y. Cao, A. Stavrinadis, T. Lasanta, D. So and G. Konstantatos, *Nat. Energy*, 2016, **1**, 16035.

7 C. T. Smith, M. A. Leontiadou, P. C. J. Clark, C. Lydon, N. Savjani, B. F. Spencer, W. R. Flavell, P. O'Brien and D. J. Binks, *J. Phys. Chem. C*, 2017, **121**, 2099–2107.

8 E. J. D. Klem, H. Shukla, S. Hinds, D. D. MacNeil, L. Levina and E. H. Sargent, *Appl. Phys. Lett.*, 2008, **92**, 212105.

9 G. Wittstock, I. Kartio, D. Hirsch, S. Kunze and R. Szargan, *Langmuir*, 1996, **12**, 5709–5721.

10 A. H. Ip, S. M. Thon, S. Hoogland, O. Voznyy, D. Zhitomirsky, R. Debnath, L. Levina, L. R. Rollny, G. H. Carey, A. Fischer, K. W. Kemp, I. J. Kramer, Z. Ning, A. J. Labelle, K. W. Chou, A. Amassian and E. H. Sargent, *Nat. Nanotechnol.*, 2012, **7**, 577–582.

11 B. F. Spencer, M. A. Leontiadou, P. C. J. Clark, A. Williamson, M. G. Silly, F. Sirotti, S. M. Fairclough, D. C. J. Neo, A. A. R. Watt and W. R. Flavell, *Appl. Phys. Lett.*, 2016, **108**, 091603.

12 M. R. Dewi, G. Laufersky and T. Nann, *RSC Adv.*, 2014, **4**, 34217.

13 L. V. Yashina, A. S. Zyubin, R. Püttner, T. S. Zyubina, V. S. Neudachina, P. Stojanov, J. Riley, S. N. Dedyulin, M. M. Brzhezinskaya and V. I. Shtanov, *Surf. Sci.*, 2011, **605**, 473–482.

14 A. Lobo, T. Möller, M. Nagel, H. Borchert, S. G. Hickey and H. Weller, *J. Phys. Chem. B*, 2005, **109**, 17422–17428.

15 D. J. H. Cant, K. L. Syres, P. J. B. Lunt, H. Radtke, J. Treacy, P. J. Thomas, E. A. Lewis, S. J. Haigh, P. O. Brien, K. Schulte, F. Bondino, E. Magnano and W. R. Flavell, *Langmuir*, 2015, **31**, 1445–1453.

16 L. Kronik and Y. Shapira, *Surf. Sci. Rep.*, 1999, **37**, 1–206.

17 L. Kronik and Y. Shapira, *J. Vac. Sci. Technol. A Vacuum, Surfaces, Film.*, 1993, **11**, 3081.

18 E. Beyreuther, J. Becherer, A. Thiessen, S. Grafstr and L. M. Eng, *Surf. Sci.*, 2013, **612**, Pages 1-9.